

# Clustering on very small scales from a large sample of confirmed quasar pairs: Does quasar clustering track from Mpc to kpc scales?

S. Eftekharzadeh<sup>1</sup>, A. D. Myers<sup>1</sup>, J. F. Hennawi<sup>2,3</sup>, S. G. Djorgovski<sup>4</sup>, G. T. Richards<sup>5</sup>, A. A. Mahabal<sup>6</sup>, M. J. Graham<sup>4,7</sup>

<sup>1</sup> Department of Physics and Astronomy, University of Wyoming, 1000 University Ave., Laramie, WY, 82071

<sup>2</sup> Max-Planck-Institut für Astronomie, Heidelberg, Germany

<sup>3</sup> Department of Physics, Broida Hall, University of California, Santa Barbara, CA 93106-9530

<sup>4</sup> Astronomy Department, California Institute of Technology, 1200 East California Boulevard, Pasadena, CA, 91125

<sup>5</sup> School of Physics and Center for Relativistic Astrophysics, Georgia Institute of Technology, 837 State Street NW, Atlanta, GA 30332-043.

<sup>6</sup> Cahill Center for Astronomy and Astrophysics, California Institute of Technology, 1200 E California Blvd, MC 249-17, Pasadena CA, 91125

<sup>7</sup> National Optical Astronomy Observatory, 950 N Cherry Avenue, Tucson, AZ 85719

30 July 2021

## ABSTRACT

We present the most precise estimate to date of the clustering of quasars on very small scales, based on a sample of 47 binary quasars with magnitudes of  $g < 20.85$  and proper transverse separations of  $\sim 25 h^{-1}$  kpc. Our sample of binary quasars, which is about 6 times larger than any previous spectroscopically confirmed sample on these scales, is targeted using a Kernel Density Estimation technique (KDE) applied to Sloan Digital Sky Survey (SDSS) imaging over most of the SDSS area. Our sample is “complete” in that all of the KDE target pairs with  $17.0 \lesssim R \lesssim 36.2 h^{-1}$  kpc in our area of interest have been spectroscopically confirmed from a combination of previous surveys and our own long-slit observational campaign. We catalogue 230 candidate quasar pairs with angular separations of  $< 8''$ , from which our binary quasars were identified. We determine the projected correlation function of quasars ( $\bar{W}_p$ ) in four bins of proper transverse scale over the range  $17.0 \lesssim R \lesssim 36.2 h^{-1}$  kpc. The implied small-scale quasar clustering amplitude from the projected correlation function, integrated across our entire redshift range, is  $A = 24.1 \pm 3.6$  at  $\sim 26.6 h^{-1}$  kpc. Our sample is the first spectroscopically confirmed sample of quasar pairs that is sufficiently large to study how quasar clustering evolves with redshift at  $\sim 25 h^{-1}$  kpc. We find that empirical descriptions of how quasar clustering evolves with redshift at  $\sim 25 h^{-1}$  Mpc also adequately describe the evolution of quasar clustering at  $\sim 25 h^{-1}$  kpc.

**Key words:** cosmology: observations, large-scale structure of universe; quasars: general, surveys

## 1 INTRODUCTION

Quasars, like galaxies, are biased tracers of the underlying dark matter distribution (e.g., Cole & Kaiser 1989; Berlind & Weinberg 2002). Many models invoke galaxy mergers as the mechanism for triggering quasar activity, although the necessity of such a mechanism is still debated (e.g., Coil et al. 2007; Padmanabhan et al. 2009; Green et al. 2011). Certainly, though, structure formation models can reproduce quasar demographics under the assumption that quasar activity is triggered by mergers (e.g., Wyithe & Loeb 2005). The peaks of the density field in which quasars reside might have been particularly strongly clustered, given that mergers are more frequent in denser environments (e.g., Kaiser 1984; Lacey & Cole 1993; Di Matteo, Springel & Hernquist 2005;

Hopkins et al. 2008) and that density signals from mergers can persist on timescales similar to the lifetime of quasars (Wetzell, Cohn & White 2009). Quasar clustering measurements therefore offer a tool by which to understand the physical processes that trigger quasar activity. The ongoing attempts to conduct such investigations become more challenging at higher luminosities (e.g., Ellison et al. 2011, 2013; Jiang et al. 2016).

Surveys such as the Sloan Digital Sky Survey (SDSS), increased the sample size and number density of quasars in a large volume of space, substantially improving measurements of quasar clustering on large or “two-halo” scales (e.g., Porciani, Magliocchetti & Norberg 2004; Croom et al. 2005; Myers et al. 2006; Porciani & Norberg 2006; Myers et al. 2007a; Shen et al. 2007, 2009; Ross et al. 2009; White et al. 2012;

Eftekharzadeh et al. 2015). Measuring quasar clustering on small scales, however, is more challenging for several reasons. First, quasars with small angular separations ( $< 60''$ ) are simply rare. Second, surveys that use fiber-fed multi-object spectrographs, such as the SDSS, prevent fibers from colliding by never placing two fibers closer than about  $60''$  on a single plate (Blanton et al. 2003; Dawson et al. 2013). Third, finding rare quasar pairs without exploiting large surveys typically requires many individual long-slit observations of pairs of candidates, which is time-consuming.

The first small-scale quasar pairs were often discovered by chance in dedicated fields, or during long-slit surveys for gravitationally lensed quasars<sup>1</sup> (e.g., Sramek & Weedman 1978; Weedman et al. 1982; Crampton et al. 1988; Hewett et al. 1989; Meylan & Djorgovski 1989; Schneider, Schmidt & Gunn 1994; Hagen et al. 1996; Fan et al. 1999; Kochanek, Falco & Muñoz 1999; Mortlock, Webster & Francis 1999; Schneider et al. 2000; Gregg et al. 2002; Miller et al. 2004; Pindor et al. 2006; McGreer et al. 2016). Although the search for high redshift quasar pairs dates back to individual discoveries of quasars at  $z \sim 4$  (e.g., Crampton et al. 1988; McCarthy et al. 1988; Meylan et al. 1990; Djorgovski 1991; Schneider, Schmidt & Gunn 1994; Hewett et al. 1998; Zhdanov & Surdej 2001), with the development of photometric selection algorithms to build homogeneous sets of quasar candidates from large imaging surveys (e.g., Richards et al. 2004, 2009), it became possible to conduct more homogeneous searches by prioritizing highly-probable close quasar pairs and following them up with long-slit spectroscopic surveys (e.g., Hennawi et al. 2006b; Myers et al. 2007b, 2008). These surveys focused on quasar pairs separated by less than  $2000 \text{ km s}^{-1}$  in redshift-space in order to measure small-scale clustering, denoting such pairs “binary quasars,” a term that has appeared for decades in the literature (e.g. Muñoz et al. 1998). Hennawi et al. (2006b) elucidate the specific use of a velocity range of  $|\Delta v| < 2000 \text{ km s}^{-1}$  as being wide enough to cover the most prominent sources of redshift uncertainty for quasars. In particular, peculiar velocities of up to  $500 \text{ km s}^{-1}$  in dense environments and blueshifted broad lines of up to  $1500 \text{ km s}^{-1}$  (Richards et al. 2002; Hennawi et al. 2006b).

In tandem with similar homogeneous searches for gravitational lenses (Oguri et al. 2006, 2008; Inada et al. 2008, 2010; Oguri et al. 2012; Inada et al. 2012) work on binary quasars has driven measurements of quasar clustering on very small scales down below even a few hundred kiloparsecs ( $\sim 10''$  or lower). For example, Kayo & Oguri (2012) took advantage of the Sloan Digital Sky Survey Quasar Lens Search (Inada et al. 2012), to measure the quasar correlation function down to  $\sim 10 h^{-1} \text{ kpc}$ .

In this paper, we continue in the vein of Hennawi et al. (2006b), Myers et al. (2007b) and Myers et al. (2008). We identify high-probability candidate close quasar pairs from a homogeneous catalogue of candidates and follow them up with confirming spectroscopy. Our target sample is drawn from quasar candidates selected using Kernel Density Estimation (KDE) by Richards et al. (2009). This “KDE” sample is not only large, it is pure<sup>2</sup>, so presents an efficient parent sample to mine for binary quasars. The sample of 47 confirmed binary quasars that we will discuss in this paper is complete for angular separations of  $2.9'' < \theta < 6.3''$  and redshifts

of  $0.43 < z < 2.26$ . Note that we will use the term “complete” here, to refer to 100% confirmation of whether or not all of our candidate target pairs are a binary quasar. We do not mean complete in the sense of also capturing quasars that are *not in* the KDE catalogue. Our sample improves on previous work in being over five times larger than previous samples of binaries on the range of scales that we cover ( $\sim 20 - 40 h^{-1} \text{ kpc}$ ). The  $> 2\times$  more precise correlation function that we calculate over proper separations at  $< 50 h^{-1} \text{ kpc}$  is therefore the tightest constraint on quasar clustering to date on scales of a few tens of kiloparsecs.

This paper is structured as follows: The data are introduced in §2, and our methodology for measuring and modeling clustering is discussed in §3.1. §4 is dedicated to the interpretation of our clustering results, before we summarize our work in §5. We adopt a  $\Lambda$ CDM cosmological model with  $\Omega_m = 0.307$ ,  $\Omega_\Lambda = 0.693$ ,  $h = 0.677$  consistent with Planck Collaboration et al. (2015). All distances quoted throughout the paper are in proper coordinates unless mentioned otherwise. We convert measurements from the literature to proper coordinates prior to comparing such measurements to our results. We use “cMpc” and “ckpc” to denote comoving distance units when we compare our measurements in proper coordinates to correlation lengths in comoving coordinates that have been derived from Mpc-scale clustering measurements. In our chosen cosmology, an angular separation of  $1''$  at  $z = 1.5$  corresponds to a proper separation of  $5.9 h^{-1} \text{ kpc}$ .

## 2 DATA

### 2.1 Identification of new quasar pairs

Our starting sample consists of 1,172,157 high-probability candidate quasars identified by Richards et al. (2009) using Kernel Density Estimation (henceforth KDE; see also Richards et al. 2004). Richards et al. (2009) applied the KDE technique to a test sample consisting of all point sources in SDSS Data Release 6 (DR6; Adelman-McCarthy et al. 2008) imaging down to a limiting magnitude of  $i = 21.3$ . These test data were labeled as a “star” or a “quasar” using a non-parametric Bayesian classifier, based on their position in *ugriz* colour space. The PSF-magnitudes of the sources were extinction-corrected based on the Schlegel, Finkbeiner & Davis (1998) dust maps. The density of the “quasar” and “star” colour space was established by applying the KDE technique to “training” samples of stars and quasars. The “stars” training set resembled a randomly drawn subset of the test set. The “quasars” training set consisted of spectroscopically confirmed SDSS quasars (Schneider et al. 2007) largely limited to  $i < 19.1$  at  $z < 3$  and  $i < 20.2$  at  $z > 3$ . At higher redshift, the quasar training sample was supplemented by quasars from the AAOmega-UKIDSS-SDSS (AUS) QSO survey (Croom et al., in prep) and from Fan et al. (2006). Given that the position of the quasar locus in colour space relative to that of the stellar locus changes significantly with redshift, Richards et al. (2009) conducted a redshift-and-colour-based sub-classification in four narrower ranges of; low redshift ( $z \leq 2.2$ ); intermediate redshift ( $2.2 \leq z \leq 3.5$ ); high redshift ( $z \geq 3.5$ ); and also UV-excess (UVX), based on  $u - g$  colour. High-probability quasars classified in these ranges are denoted `lowzts==1`, `midzts==1`, `hizts==1` or `uvxts==1`, respectively (see Table 2 of Richards et al. 2009).

From the initial KDE sample of 1,172,157 candidate quasars, we sub-selected candidates that are brighter than 20.85 in (Galactic-extinction-corrected) *g*-band and are categorized as

<sup>1</sup> SDSS J1637+2636AB was the first binary QSO discovered, but originally misinterpreted as a lens (Djorgovski & Spinrad 1984). Due to this misinterpretation, the quasar pair PKS 1145-071 was initially known as the first binary quasar (Djorgovski et al. 1987).

<sup>2</sup>  $> 90\%$  of KDE candidates at  $0.4 \lesssim z \lesssim 2.3$  are expected to be quasars

$hizts==1$  OR  $uvxts==1$ . We further restricted this subsample to the  $70^\circ < \text{RA} < 300^\circ$  region of the DR6 imaging footprint, resulting in a total of 369,559 quasar candidates. We will hereafter refer to these 369,559 candidates as our “parent sample”. We cross-matched the candidates by angular separation and identified 230 candidate pairs with separations of  $2.8'' < \theta < 8''$ . Here, the upper limit is chosen to correspond to a few hundred kpc for likely quasar redshifts. The lower limit is chosen to match roughly twice the seeing of the SDSS imaging data (e.g. see Figure 4 of Abazajian et al. 2003) in order to protect against sources that are merged in SDSS imaging.

To determine which of our candidate pairs had already been identified as quasars, we used a radius of  $1''$  to cross-match our parent sample with previously known, spectroscopically confirmed, visually inspected, quasars. These “known” quasars were drawn from programs conducted to identify quasar pairs (Hennawi et al. 2006a,b; Myers et al. 2008; Hennawi et al. 2010; Hennawi & Prochaska 2013; Prochaska et al. 2013; Prochaska, Lau & Hennawi 2014) and gravitational lenses (Oguri et al. 2008, 2012; Inada et al. 2008, 2012) as well as SDSS Data Release 7 (DR7; Schneider et al. 2010) and Data Release 12 (DR12; Pâris et al. 2016, henceforth DR12Q). In particular, DR12Q includes objects from an SDSS ancillary program designed specifically to target some of our candidate quasars<sup>3</sup>. We then identified candidate quasar pairs that did not have *both* members of the pair previously spectroscopically confirmed, and reserved such ( $2.8'' < \theta < 8''$ ) pairs for further spectroscopic confirmation.

Long-slit spectroscopy of these selected candidate quasar pairs was conducted on a range of facilities outlined in Table 1, with the slit oriented to observe both quasars simultaneously. The spectra were reduced and calibrated using the XIDL package<sup>4</sup>. Figures 1 and 2 show three examples of reduced spectra of our quasar pairs. Table 5 contains the full list of 230 candidate quasar pairs drawn from our parent sample, together with available spectroscopic confirmations and redshifts from our own and previous campaigns.

## 2.2 A KDE-complete sample of binary quasars

Our goal is to characterize quasar clustering on very small scales using a statistically uniform sample of quasars that are proximate to each other (so-called “binary” quasars). Following Hennawi et al. (2006b). We designate pairs of quasars that do not meet this criterion to be “projected pairs.” Over the course of our campaign to date, we have obtained definitive classifications for a close to complete sample of KDE-selected candidates on angular scales of  $2.9'' \leq \theta \leq 7.7''$ , which correspond to proper scales<sup>5</sup> of roughly  $15 \leq R \leq 40 h^{-1}$  kpc over the main redshift range of our sample. The resulting sample consists of 169 candidate quasar pairs, which we will refer to as our sample of “relevant pairs”. Note that good spectroscopy of *both* candidates is not required to “definitively classify” a pair as *not* a binary quasar. For instance, if one of a pair of objects is categorically identified as a star or a galaxy, then that pair is a non-binary, and we classify it as a “projected pair.” Further, if a known quasar at a redshift of  $z$  has a companion for which we have a spectrum that is of sufficiently high quality that we

should certainly have identified broad emission lines corresponding to  $z$ , then we also classify that pair as a projected pair. Note that we do not consider confirmed quasar pairs to be “binary” even if their velocity separation is only slightly larger than  $2000 \text{ km s}^{-1}$ . In addition, we removed one pair<sup>6</sup> from our “relevant pair” sample that consisted of two high signal-to-noise but featureless (“continuum”) sources. Even if this pair is a binary quasar, we would have no way to assign it a redshift.

Table 2 records the nature of our total of 169 relevant pairs, including their ultimate classification as a binary quasar, a projected pair, a pair for which there is insufficient information to characterize it, or a gravitational lens<sup>7</sup>. The distribution on the sky of the binary quasars in our sample of relevant pairs is shown in Figure 3, against a background of all of the KDE-selected candidates in our parent sample. Our follow-up spectroscopy of candidate pairs, provided 126 *new* sets of observations of candidate quasar pairs that have separations of less than  $7.7''$ . Of these 126 newly characterized pairs, we confirmed 53 to be binary quasars. Richards et al. (2009) used clustering analyses to estimate that the KDE selection algorithm is 92.7% efficient for sources with  $hizts==1$  OR  $uvxts==1$ . If we designate as “stars” those objects in our sample that do not have a sufficiently good spectrum to classify the object<sup>8</sup>, then we find that out of the 338 sets of candidate quasars in our sample of 169 relevant pairs, we confirm 309 to be quasars. This is in excellent agreement with an efficiency of  $\sim 92.5\%$  for the KDE catalogue.

Typically, clustering studies construct a random catalogue, or otherwise analytically correct for sources of incompleteness that arise when targeting quasars (e.g. Eqn. 17 of Hennawi et al. 2006b). To circumvent incompleteness corrections when conducting clustering analyses, we instead construct a sample of pairs that we have categorically identified as either a binary quasar or not. We will henceforth refer to this subset of pairs as our “KDE-complete” sample. Binary quasars in the KDE-complete redshift and proper scale ranges can be used for clustering analyses without correcting for incompleteness in our spectroscopic campaign (because, by definition, this range is 100% complete to possible binary quasars in our parent sample). The outer limits of our KDE-complete sample in redshift and proper transverse scale are defined by the ranges at which there exist quasar pairs that we cannot categorically classify as a binary or not. Typically, this is because the spectroscopic information for either one or both members of the pair does not exist. Note that there are cases where spectroscopic confirmation of only one member of a pair is sufficient to include that pair in the KDE-complete sample. Most obviously, as also noted above, pairs that include one non-quasar have sufficient information to be included in the KDE-complete sample. In addition, though, pairs that include one confirmed quasar with a (spectroscopic) redshift that would categorically place it outside of the proper-scale range of interest can also be used to define the KDE-complete ranges, regardless of whether such a quasar’s companion has itself been spectroscopically confirmed.

Figure 4 shows the redshift and proper transverse separation ranges for binary quasars in our KDE-complete sample. The dotted lines show the transverse separations corresponding to the  $2.9'' \leq \theta \leq 7.7''$  angular range of our 169 relevant pairs. The extent of the

<sup>3</sup> <http://www.sdss.org/dr12/algorithms/ancillary/boss/smallscale/> SDSS J1336+2737 with a separation of  $5.41''$

<sup>4</sup> <http://www.ucolick.org/~xavier/IDL/index.html>

<sup>5</sup> We use the angular separation and confirmed redshift of the *brighter* member in each of our relevant pairs to calculate the proper transverse separation between members of the pair.

<sup>7</sup> We designate binary quasars as gravitational lenses if they are convincingly argued to be lenses in the literature.

<sup>8</sup> a reasonable assumption, given that quasars are much easier to classify at low-signal-to-noise as compared to stars.

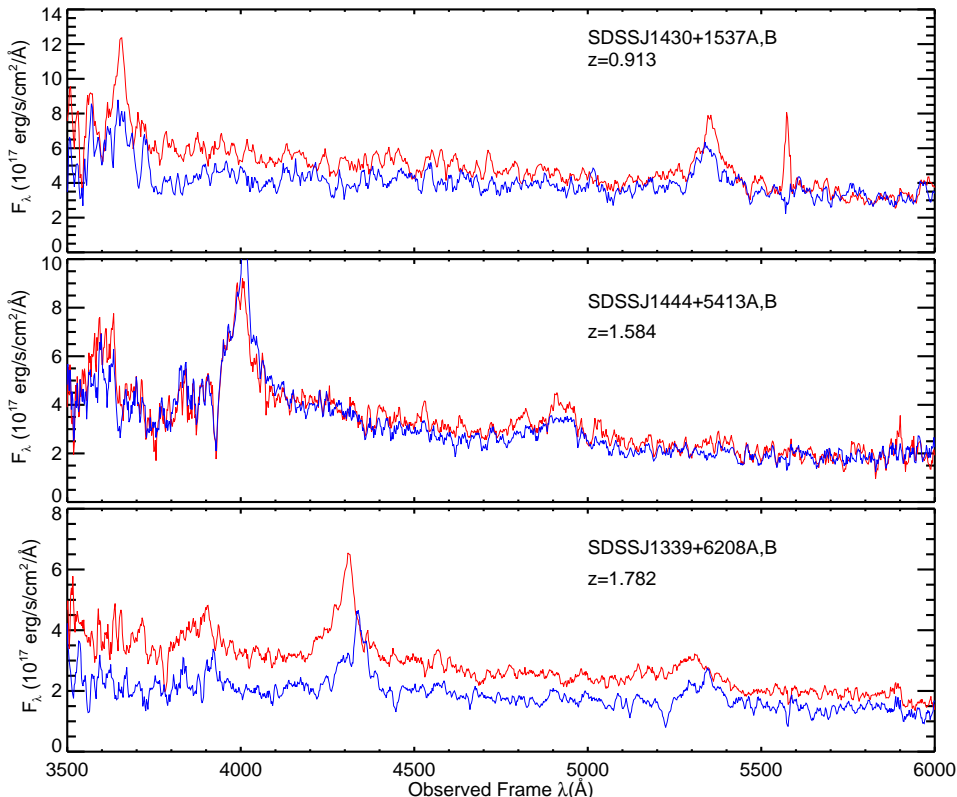


**Figure 1.** Three example spectra of confirmed binary quasars. The spectra are smoothed by 5 pixels to aid visualization.

KDE-complete sample of binaries both in redshift and in transverse separation is depicted by a grey box. This box is limited by either the angular extent of our sample of relevant pairs, or by quasar pairs that we cannot currently confirm or reject as a binary based on the spectroscopic information to hand (depicted by open circles in Figure 4). The ranges of redshift and proper separation that define the limits of the KDE-complete sample (i.e. the edges of the grey box in Figure 4) are  $0.44 \leq z \leq 2.31$  and  $17.0 \leq R \leq 36.2 h^{-1}$  kpc. Table 6 lists the sample of 47 binary quasars that define our KDE-complete sample. Figure 4 also illustrates that we only consider a small fraction of space with  $\theta < 3''$ , in keeping with the arguments in Pindor et al. (2003) and Hennawi et al. (2006b) that sources with  $\theta < 3''$  can appear blended in SDSS imaging.

### 3 METHODOLOGY

#### 3.1 Estimating the small-scale clustering of quasars

We measure the correlation function in proper coordinates, projected across a redshift window of  $< 2000 \text{ km s}^{-1}$  (our definition of a “binary quasar” from §2), using the estimator

$$\bar{W}_p = \frac{QQ}{\langle QR \rangle} - 1 \quad (1)$$

(e.g., Peebles 1973; Shanks et al. 1987; Croom & Shanks 1996). Here,  $QQ$  represents a count of quasar-quasar data pairs and  $\langle QR \rangle$  denotes the “expected” number of quasar-random pairs in a given bin of redshift, angle or proper separation. Note that

$$\langle QR \rangle = \frac{N_Q}{N_R} QR, \quad (2)$$

where  $N_Q/N_R$  is the size of the quasar catalogue compared to the size of a (larger) random catalogue. An appropriate random catalogue will mimic the angular and redshift distribution of the data, in the absence of any clustering. Since our KDE-complete sample of binary quasars is drawn from the KDE catalogue described in §2, the random catalogue needs to have the same overall angular and redshift coverage as the KDE catalogue (see, e.g., Myers et al. 2006, 2007a).

The entire volume of the KDE catalogue comprises  $\sim 41.93 (h^{-1} \text{Gpc})^3$ . Generating a sufficiently large random catalogue over such a volume purely for the purposes of making a kpc-scale clustering measurement is a computationally expensive task. Such an approach is also unnecessary, as we only seek  $QR$  pairs with small angular separations ( $\leq 7.7''$ ). We therefore construct a random catalogue for our analysis using three independent steps. As our sample of pairs is complete for proper scales of  $17.0 \leq R \leq 36.2 h^{-1}$  kpc (see §2), these three steps are sufficient to model the expected, unclustered distribution of our sample of binary quasars:

(1) We randomly selected a subset of  $N_Q = 342,581$  KDE candidate quasars, corresponding to 92.7% of our parent sample of 369,559 KDE candidates (see §2). This down-sampling is necessary because the efficiency of the KDE algorithm for selecting our overall sample of candidate quasars (`lowzts` and `uvxts`; again see §2) is  $\sim 92.7\%$ .

We randomly generated positions around these 342,581 KDE

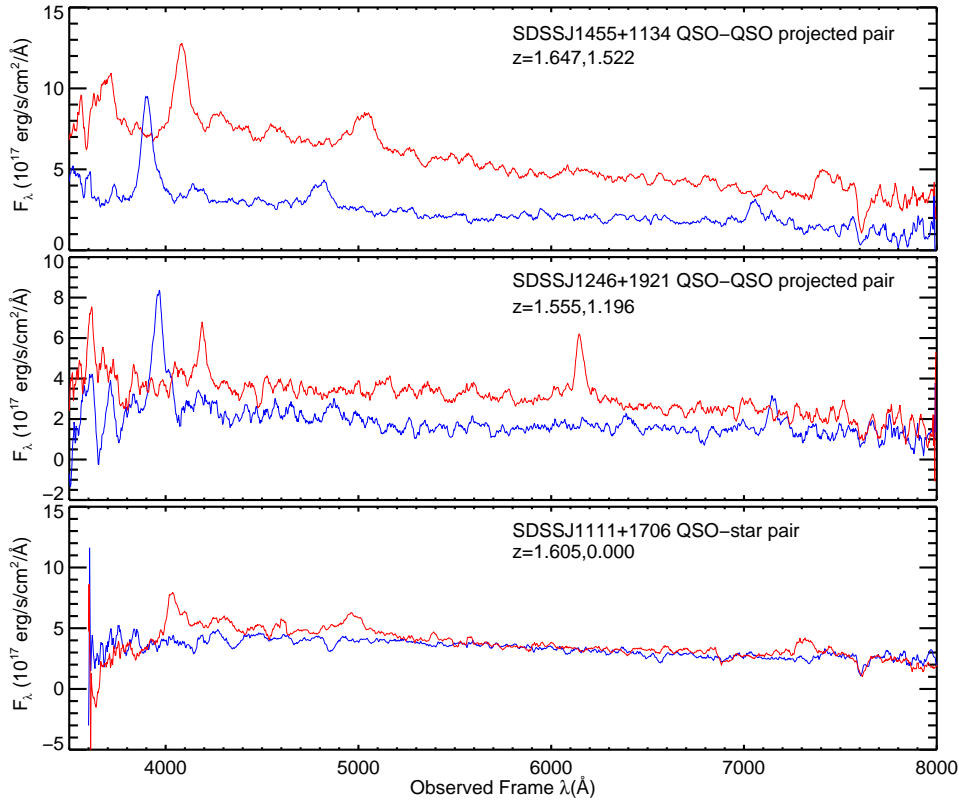


**Figure 2.** Three example spectra of quasar pairs that are not binaries. Such pairs can be two quasars that are aligned along the line of sight but have different redshifts, star-quasar pairs, or star-star pairs.

Telescope	Instrument	Spectrograph Type	Spectral Coverage ( $\text{\AA}$ )	FWHM	Dates	Reference
Mayall 4-m	Ritchey-Chrétien Spectrograph (RC)	Single	3600 – 9200	325	9-11 Feb., 7-10 Jun. 2008	(1)
Palomar 200 inch	Double Spectrograph (DBSP)	Double	3100 – 9300	900/550	28-29 Feb., 2-5 Apr. & 4-6 May 2008	(2)
Palomar 200 inch	Double Spectrograph	Double	3100 – 9300	900/550	24 Feb., 30 Mar., 27 Apr. & 17 Jun. 2009	(2)
Palomar 200 inch	Double Spectrograph	Double	3100 – 9300	900/550	7-10 Nov. 2010	(2)
Palomar 200 inch	Double Spectrograph	Double	3100 – 9300	900/550	2-3 Mar. 2011	(2)

**Table 1.** Summary of the follow-up spectroscopic campaign for a complete subsample of the KDE-selected quasar candidates. The *Reference* column refers to (1) Sheinis et al. (2002); (2) Oke & Gunn (1983).

candidate quasars on angular scales of  $2.9'' < \theta < 7.7''$ , which is the range of angular separations of candidate quasar pairs on our “KDE-complete” scales of interest (see §2 and, specifically Figure 4). We will refer to the resulting catalogue as our *angular* random catalogue.

(2) Only  $\sim 36\%$  (131,928) of the KDE candidates have a confirmed spectroscopic redshift. We used the *full* distribution of spectroscopic redshifts in the KDE sample, displayed in Figure 5, and randomly drew redshifts from the resulting  $dN/dz$  for both those candidates with no spectroscopic redshift and for objects in our angular random catalogue. Then, working with quasars with redshifts within our range of interest ( $0.43 < z < 2.26$ ), we down-sampled our angular random catalogue by retaining only random points in  $QR$  pairs separated by  $< 2000 \text{ km s}^{-1}$  (our definition of a “binary quasar” from §2). We will refer to the resulting catalogue as our *redshift* random catalogue.

(3) Using the redshift and angular separation information that we generated in steps (1) and (2), we further limited our redshift random catalogue to only  $QR$  pairs that intersected with the limits in redshift and proper scale of our “KDE-complete” sample of binary quasars (see Figure 6). We will refer to the resulting catalogue as our *final* random catalogue. A total of 290,694 KDE candidate quasars have spectroscopic redshifts in the range of our complete sample of binary quasars ( $0.43 < z < 2.2$ ). The final random catalogue (“ $R$ ”) can be used in conjunction with these 290,694 KDE candidate quasars (“ $Q$ ”) to calculate  $QR$  in Eqn. 2 as a function of scale or redshift.

The steps that produce the redshift and final random catalogues discard points that do not create eligible  $QR$  pairs. It is therefore necessary to generate a large enough initial angular random catalogue to retain a sufficiently large final random catalogue with which to infer  $\langle QR \rangle$ . We found that assigning each of the

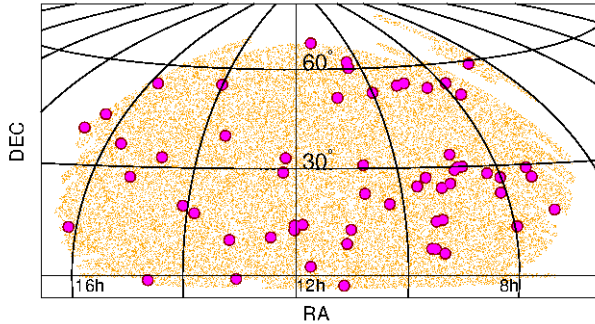


**Figure 3.** Coordinates of the 369,559 quasar candidates in our parent sample (orange) in Aitoff projection. The filled circles depict the 58 spectroscopically confirmed binaries in our sample of relevant pairs. The data have been cut to the NGC imaging footprint of SDSS DR6, our main area of focus.

Category	# of pairs
Confirmed binaries	58
Confirmed lenses	5
Confirmed quasar pairs (non-binaries)	77
Pairs with at least one confirmed non-quasar member	8
Pairs with at least one unknown member	21

**Table 2.** Classification of all 169 “relevant pairs” in our sample (with  $g < 20.85$  and  $2.9'' < \Delta\theta < 7.7''$ ). “Confirmed binaries” meet the classification of a binary quasar for the purposes of this paper ( $|\Delta v| < 2000 \text{ km s}^{-1}$  and not otherwise identified as a gravitational lens); “Confirmed quasar pairs” denotes pairs for which we have spectroscopic information for both members of the candidate pair and that have  $|\Delta v| \geq 2000 \text{ km s}^{-1}$ .

$\Delta z$	$(1/N) dN/dz$
0.43	0.191
0.44	0.239
0.45	0.200
0.46	0.230
0.47	0.240
0.48	0.225
0.49	0.239
0.50	0.284
0.51	0.288
0.52	0.288
0.53	0.305
0.54	0.308
0.55	0.258
0.56	0.339
0.57	0.303
0.58	0.322
0.59	0.389
0.60	0.366
0.61	0.398
0.62	0.385

**Table 3.** Normalized distribution of the spectroscopic redshifts of quasars in our parent sample of candidates. The full table is available in the electronic version of this paper.

290,694 KDE candidate quasars in our redshift range of interest  $N = 2000$  random points on scales of  $0'' < \theta < 7.7''^9$  was sufficient in this regard, as such a schema ultimately provided more than 20 random points around each KDE candidate quasar. Essentially, this means that our *final* random catalogue is at least  $20\times$  larger than our data catalogue.

An important consideration is that the  $N_R$  in Eqn. 2 does not denote the  $N = 2000$  random points that we generated around each of the  $N_Q = 290,694$  KDE candidate quasars in our redshift range of interest. Rather, it corresponds to the number of random points that would have truly been generated, had we chosen to populate the *entire survey volume*. We calculate  $N_R$  as the “populated areal number density of the random points”  $\times$  “the full area of the survey footprint”:

$$N_R = \frac{N}{A(< 7.7'')} A_{\text{full}}, \quad (3)$$

where  $N = 2000$  is the number of random points we generated around each candidate quasar to  $\theta < 7.7''$ ,  $A(< 7.7'')$  is the survey area within  $7.7''$  of a candidate quasar and  $A_{\text{full}}$  is the full area of the survey footprint (the orange footprint in Figure 3).

To calculate the survey area, we use the SDSS “survey coordinates”,  $\eta$  and  $\lambda$  (e.g. Stoughton et al. 2002), to construct stripe-shaped polygons along great circles using the MANGLE software (Blanton et al. 2003; Tegmark et al. 2004; Swanson et al. 2008). We also create “holes” in the footprint corresponding to SDSS imaging masks<sup>10</sup>. Note that when we created the angular random catalogue, we discarded any points that lay in holes or outside of the survey area, but this made very little difference on scales of  $\theta < 7.7''$ . Based on this process, the total area of the survey footprint that is used in this study is  $A_{\text{full}} = 7600.4 \text{ deg}^2$ . Since we only consider angular scales up to  $7.7''$  the “effective” area around any individual candidate quasar is  $A(< 7.7'') = 1.44 \times 10^{-5} \text{ deg}^2$ . So,  $N_R = (2000 \times 7600.4) / 1.44 \times 10^{-5} \sim 10^{12}$ . In other words, the process that we have outlined would be equivalent to generating a very, very large random catalogue across the entire survey volume.

### 3.2 Theoretical Considerations

The volume averaged projected correlation function ( $\bar{W}_p$ ) is a useful estimator for our purposes given the large volume occupied by quasars over a wide redshift range, compared to the small scales on which we seek to measure clustering.  $\bar{W}_p$  can be converted to the more common clustering estimators used on large scales via the formalism presented in, e.g., Hennawi et al. (2006b).

The projected real-space correlation function of quasars with a maximum velocity difference of  $|\Delta v| < 2000 \text{ km s}^{-1}$  can be interpreted as :

$$w_p(R, z) = \int_{-v_{\text{max}}/H(z)}^{v_{\text{max}}/H(z)} \xi_s(R, s, z) ds, \quad (4)$$

where  $v_{\text{max}} = 2000 \text{ km s}^{-1}$ ,  $H(z)$  is the expansion rate at redshift  $z$  and  $\xi_s$  is the quasar correlation function in redshift-space.

As discussed in Hennawi et al. (2006b), it is a good approximation to replace the redshift-space correlation function  $\xi_s$  with

<sup>9</sup> We assigned 2000 points over  $\theta < 7.7''$  and then clipped them to cover  $2.9'' < \theta < 7.7''$ , to provide flexibility if our minimum angle changed.

<sup>10</sup> e.g., <http://classic.sdss.org/dr6/products/images/index.html>

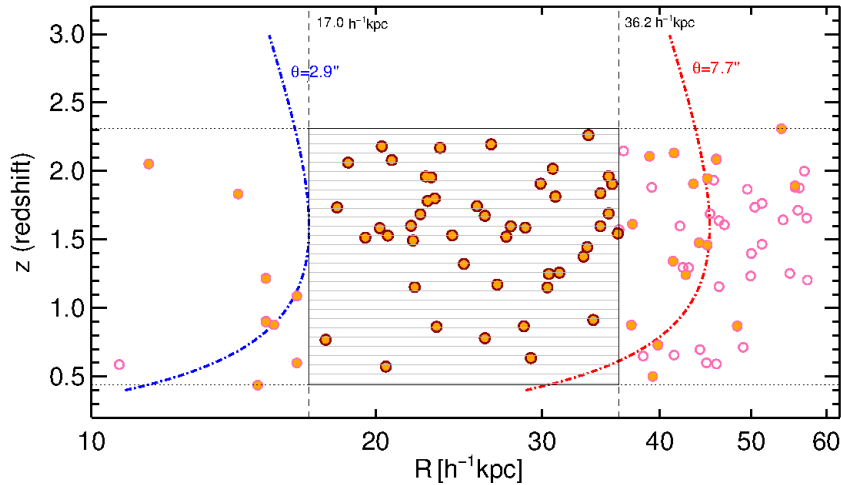


**Figure 4.** Redshift and proper transverse separation range probed by the binary quasars in our “KDE-complete” sample. Filled circles represent spectroscopically confirmed binary quasars. Open circles represent binary quasars for which spectroscopic information exists for only one of the members of the pair. The dotted lines depict transverse separations corresponding to  $2.9'' \leq \theta \leq 7.7''$ , the angular range of our 169 relevant candidate quasar pairs. The extent of our “KDE-complete” sample of 47 binaries is depicted by a grey box that is limited by either the angular extent of our sample of relevant pairs, or by quasar pairs that we cannot currently confirm or reject as a binary based on spectroscopy.

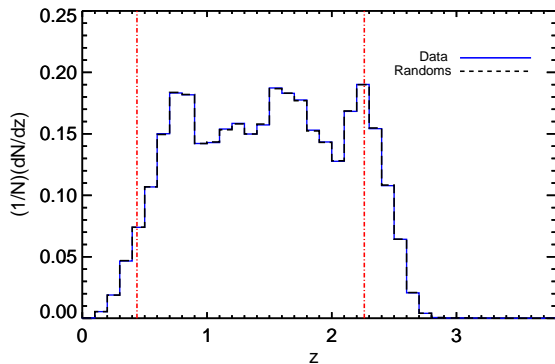


**Figure 5.** The normalized redshift distribution of spectroscopically confirmed quasars in our sample of relevant pairs (blue solid line), compared to the generated distribution for our redshift random catalogue (black dashed line). The vertical red dot-dashed lines delineate the redshift range of the KDE-complete sample.

its three-dimensional real-space counterpart  $\xi(r)$ . We measure the volume-averaged correlation function  $\bar{W}_p(R_{\min}, R_{\max}, z)$  (abbreviated to  $\bar{W}_p(z)$ ), by integrating over the entire radial bin of proper distance  $[R_{\min}, R_{\max}]$

$$\bar{W}_p(z) = \frac{\int_{-v_{\max}/H(z)}^{v_{\max}/H(z)} \int_{R_{\min}}^{R_{\max}} \xi(R, x, z) 2\pi R dR ds}{V_{\text{shell}}} \quad (5)$$

where  $\xi(R, x, z)$  is the correlation function and  $V_{\text{shell}}$  is the volume of the cylindrical shell in redshift space over which we integrate

$$V_{\text{shell}} = \pi(R_{\max}^2 - R_{\min}^2) \left[ \frac{2v_{\max}}{H(z)} \right], \quad (6)$$

and then averaging the redshift-dependent  $\bar{W}_p$  in Eqn. 5 over the redshift distribution of quasars in our sample.

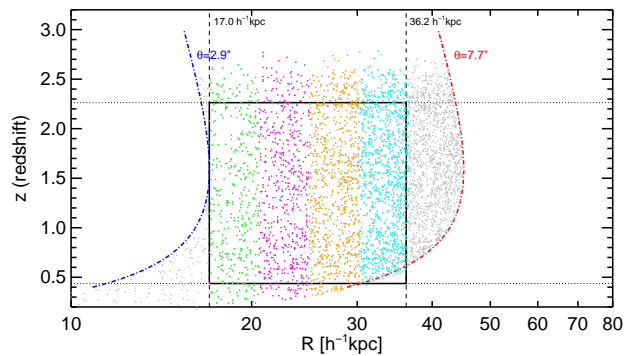


**Figure 6.** The bins in proper scale that we use in our clustering measurement are shown in different colours. This figure illustrates the difference between how the random catalogue is populated in angle and the resulting random points that are counted in bins of proper scale. The black box represents the limits of our KDE-complete sample (see also Figure 4).

We need to average  $\bar{W}_p(z)$  over the redshift distribution of our sample in a given redshift bin, in order to compare to our clustering measurement. To estimate the redshift distribution for our quasars of interest in any slice of redshift, we use the Pure Luminosity Evolution (PLE) model of Croom et al. (2009) with  $\alpha = -3.33$ ,  $\beta = -1.42$ ,  $M^* = -22.17$  and  $\log(\phi^*) = -5.84 \text{ Mpc}^{-3} \text{ mag}^{-1}$ . We adopt this particular luminosity function as the sample of quasars studied in Croom et al. (2009) is a reasonable match ( $0.4 < z < 2.6$ ) to the redshift range of our sample, and extends well beyond ( $g < 21.85$ ) our magnitude limit.

Because we measure  $\bar{W}_p$  for *quasars* the  $\xi$  included in Eqn. 5 is typically the correlation function of quasars, which we will denote  $\xi_Q$ . We will adopt two typical theoretical forms for this function. First, a two-parameter power-law of the form

$$\xi_Q(r) = (r/r_0)^{-\gamma} \quad (7)$$

where  $r_0$  is the *correlation length*, defined as the most common (probable) separation between two quasars in the sample, and  $\gamma$  is the exponent that best recreates the shape of quasar clustering. Second,

$$\xi_Q(r) = A \xi(r) \quad (8)$$

where  $A$  is the ratio of the clustering amplitude of quasars to that of the underlying dark matter distribution and  $\xi(r)$  is the correlation function of underlying dark matter, for which we adopt the model of Smith et al. (2003). In some places in §4, we use values of  $r_0$  and  $\gamma$ , or a form for  $\xi(r)$ , that have been derived for the clustering of quasars or dark matter on Mpc-scales. We then use Eqn. 5 to project this Mpc-scale result down to our kpc-scales of interest.

Phenomenologically, the formalism of Eqn. 8 resembles that for the bias of tracers of dark matter (e.g., Kaiser 1984). We appreciate, though, that small-scale bias could change rapidly with scale, and that the amplitude of quasar clustering is likely to be a complex function of several factors on non-linear scales. Any association we make between the parameter  $A$  and the bias of dark matter ( $b_Q$ ) in this work, therefore, is only for to make comparisons between the amplitude of quasar clustering at kpc- and Mpc-scales. In essence, we adopt Eqn. 8 only as an empirical parameterization of the amplitude of quasar clustering on kpc-scales. We reserve models that have a more complex physical interpretation for a later paper.

## 4 RESULTS AND DISCUSSION

Our KDE-complete sample of confirmed binary quasars is  $\sim 6$  times larger than any individual previous sample, allowing us to measure the scale-dependence of quasar clustering at  $\lesssim 40 h^{-1}$  kpc with unparalleled precision. In addition, our large sample extends across multiple bins in redshift that each contain about as many binary quasars as any previous sample. This allows us to study the evolution of quasar clustering on these very small scales for the first time.

### 4.1 The scale-dependence of $\bar{W}_p$ at $\lesssim 40 h^{-1}$ kpc

We measure the volume-averaged projected correlation function ( $\bar{W}_p$ ) of quasars in four bins of proper scale centered at 18.8, 22.8, 27.6 and 33.4  $h^{-1}$  kpc which contain 7, 14, 11 and 15 binary quasars, respectively. The bins were chosen to have the same width in logarithmic scale. The measured  $\bar{W}_p$  for each bin of proper separation together with the measured  $\bar{W}_p$  for the full sample at  $\bar{z} = 1.55$  and  $\bar{R} = 26.6 h^{-1}$  kpc are shown in Figure 7. Multiple past works have argued that pair counts on small scales are independent, and that clustering on these scales can be adequately described by a Poisson distribution (e.g. Shanks & Boyle 1994; Croom & Shanks 1996; Myers et al. 2006; Chatterjee et al. 2012, 2013). We therefore adopt Poisson errors from Gehrels (1986) for our measurements of  $\bar{W}_p$ .

Table 4 lists our measured  $\bar{W}_p$  in each bin of proper separation and for our full, KDE-complete sample of 47 binary quasars.

Figure 7 also compares our measurement of  $\bar{W}_p$  to previous estimates of quasar clustering on small scales at redshifts of  $0.5 \lesssim z \lesssim 2.5$ . Hennawi et al. (2006b) constructed a large, homogeneous catalogue of binary quasars from SDSS DR3 and used a sub-sample

$R$ ( $h^{-1}$ kpc)	$\bar{W}_p$
18.8	$79.8^{+43.5}_{-29.8}$
22.8	$109.1^{+38.0}_{-29.1}$
27.6	$58.0^{+23.7}_{-17.5}$
33.4	$59.2^{+19.9}_{-15.4}$
26.6	$72.28^{+15.2}_{-13.5}$

**Table 4.** The volume-averaged correlation function for the four bins of proper separation displayed in Figure 7. The last row corresponds to the full range of scales (the open blue circle in Figure 7).

of them to measure quasar clustering on small scales. The clustering sub-sample of Hennawi et al. (2006b) included 23 binary quasars on proper scales of  $10 \lesssim R \lesssim 100 h^{-1}$  kpc. Myers et al. (2008) built on this work by discovering 10 new binary quasars in the SDSS DR4 KDE catalogue, and used them to study quasar clustering on a specific range of very small proper scales ( $20 \lesssim R \lesssim 30 h^{-1}$  kpc). More recently, Kayo & Oguri (2012) compiled a sample of binary quasars from observations conducted across SDSS DR7 as part of the SDSS Quasar Lens Search (e.g. Inada et al. 2012), and used 26 binaries with comoving separations of  $10 - 200 h^{-1}$  ckpc (proper scales of  $5 \lesssim R \lesssim 100 h^{-1}$  kpc) to measure  $\bar{W}_p$ . The sample of Kayo & Oguri (2012) only shares 4 binaries with that of Hennawi et al. (2006b) and a further 2 with Myers et al. (2008). This is largely because the sample of Kayo & Oguri (2012) is more complete than the sample of Hennawi et al. (2006b), covers a larger range of scales than the sample of Myers et al. (2008), and covers a larger portion of the SDSS footprint as compared to both studies.

The sample of Kayo & Oguri (2012) contains only 4 binary quasars on scales of  $17 \lesssim R \lesssim 36 h^{-1}$  kpc, and two of these are the pairs that Kayo & Oguri (2012) incorporated from Myers et al. (2008). Further, the clustering sub-sample of Hennawi et al. (2006b) includes only 8 binary quasars on proper scales of  $17 \lesssim R \lesssim 36 h^{-1}$  kpc. Our KDE-complete sample of binary quasars is thus  $\sim 6\times$  larger than any previous statistically homogeneous sample at  $R \sim 25 h^{-1}$  kpc and so can substantially improve the accuracy of quasar clustering measurements on small scales. The blue open circle in Figure 7 shows the statistical significance of our measurement compared to recent such measurements on kpc-scales. Our KDE-complete sample is about  $4\times$  larger than all other combined samples at  $17 \lesssim R \lesssim 36 h^{-1}$  kpc. This essentially means that our results can be used to improve constraints on kpc-scale quasar clustering by a factor of 2 compared to previous work.

The real-space correlation function of quasars can be modeled by a simple power-law (see Eqn. 7). Quasars in our redshift range of interest ( $0.4 < z < 2.3$ ) have been argued to have a range of power-law indexes based on clustering measurements conducted on Mpc-scales. The sample that best matches our luminosity and redshift range ( $b_J < 20.85; 0.3 < z < 2.2$ ) is that of the 2dF QSO Redshift Survey (2QZ; Croom et al. 2004). For the 2QZ, Porciani, Magliocchetti & Norberg (2004) measured a best-fit power-law of  $\gamma = 1.53$  for  $r_0 = 4.8 h^{-1}$  cMpc, rising to  $\gamma = 1.8$  for  $r_0 = 5.4 h^{-1}$  cMpc. Ross et al. (2009) found that the clustering of brighter quasars from the SDSS ( $i < 19.1; 0.3 < z < 2.2$ ) required a steeper power-law of  $\gamma = 1.90^{+0.04}_{-0.03}$  for  $r_0 = 5.5 h^{-1}$  cMpc. The red dashed and blue dot-dashed lines in Figure 7 compare the best-fit power laws from



Porciani, Magliocchetti & Norberg (2004) to our results, and it is clear that our data necessitate a much steeper power-law. Fixing the correlation length to  $r_0 = 5 h^{-1}$  cMpc, we use a maximum likelihood fitting procedure to determine that our data require a power-law index of  $\gamma = 1.97 \pm 0.03$ , which is plotted as the purple dashed line in Figure 7. This power-law index is far in excess of the results of Porciani, Magliocchetti & Norberg (2004) but is in reasonable agreement with the Mpc-scale clustering of substantially brighter SDSS quasars from Ross et al. (2009). Our results also support the study of Kayo & Oguri (2012), who found a power-law of  $\gamma = 1.92 \pm 0.04$  for  $r_0 = 5.4 h^{-1}$  cMpc from a study of the clustering of bright ( $i < 19.1; 0.6 < z < 2.2$ ) SDSS quasars on proper scales of  $4 \lesssim R \lesssim 85 h^{-1}$  kpc.

At low redshift ( $z \sim 0.5$  and below), quasars appear to be roughly unbiased (e.g. Croom et al. 2005), and cluster similarly to  $L^*$  galaxies. Given that quasars are thought to be merger-driven (e.g. Hopkins et al. 2006, 2007), it is interesting to compare the overall shape of the correlation function of galaxies and of quasars at similar redshift. Any excess in quasar clustering compared to galaxies might indicate that quasars ignite in particularly grouped or “merger-prone” environments (again see Hopkins et al. 2007). For example, Watson et al. (2010) suggest that enhanced quasar activity by mergers might be responsible for the shape differences between the correlation function of Luminous Red Galaxies (LRGs) and quasars on very small scales. Large spectroscopic galaxy surveys are now approaching  $z \sim 1$ , so it is becoming realistic to compare quasar and galaxy correlation functions in similar redshift ranges.

Recent galaxy clustering results on Mpc-scales, tend to find power-law slopes that are shallower than  $\gamma = 2$ . For example, Favole et al. (2016) find  $\gamma = 1.6 \pm 0.1$  in redshift-space for  $s_0 = (5.3 \pm 0.2) h^{-1}$  cMpc for Emission Line Galaxies at  $z \sim 0.8$ . Coil et al. (2016) find a range of power-law slopes for blue and red galaxies from the PRIMUS survey over the redshift range  $0.4 \lesssim z \lesssim 0.9$ . For populations that have  $r_0$  consistent (within their  $1\text{-}\sigma$  errors) with  $5 h^{-1}$  cMpc Coil et al. (2016) find  $\gamma = 1.6 - 1.7$ , with an error less than  $\pm 0.1$ . On smaller scales, galaxy clustering may steepen, however. Masjedi et al. (2006) tracked the clustering of  $z \sim 0.25$  SDSS LRGs down to scales of  $\sim 10 h^{-1}$  kpc and estimated  $\gamma \sim 2.0$ , although they also found a large correlation length of  $r_0 \sim 10 h^{-1}$  cMpc. Zehavi et al. (2011) found power-law slopes ranging from  $\gamma \sim 1.8 - 2.0$  for  $r_0 \sim 4.5 - 10.4 h^{-1}$  cMpc down to comoving distances of  $\sim 100 h^{-1}$  ckpc for SDSS galaxies at  $z \lesssim 0.25$ . For samples that have  $r_0$  in the range  $4.5 - 5.5 h^{-1}$  cMpc Zehavi et al. (2011) find  $\gamma \sim 1.8 - 1.9$ . More recently and at higher redshift, Zhai et al. (2016) find  $\gamma \sim 1.95$  down to scales of  $\sim 300 h^{-1}$  ckpc for the clustering of  $z \sim 0.7$  LRGs drawn from the SDSS-IV/extended Baryon Oscillation Spectroscopic Survey (eBOSS). Our inferred power-law of  $\gamma = 1.97 \pm 0.03$  for  $r_0 = 5 h^{-1}$  cMpc is therefore at the steeper end of what has been measured for galaxies, but is not inconsistent with measurements at higher redshift that sample smaller scales. A detailed theoretical analysis, such as the Halo Occupation Distribution (HOD; Berlind & Weinberg 2002) formalism, should be able to use our measurements to better quantify whether quasar clustering exceeds galaxy clustering on kpc-scales, or whether quasars occupy similar halos to certain types of galaxies. We defer such a detailed HOD analysis to a later paper.

## 4.2 Redshift dependence of $\bar{W}_p$

Measurements of the evolution of quasar clustering on Mpc scales (e.g. Croom et al. 2005), in combination with the quasar luminosity function, have helped to constrain fueling models for quasars and provided a framework to link quasar activity to galaxy formation (see, e.g., Hopkins et al. 2007, and references therein). Broadly, the quasar correlation length on Mpc-scales does not appear to evolve by more than a factor of  $\sim 2$  over the range  $0.5 \lesssim z \lesssim 2.5$  (see, e.g., Eftekharzadeh et al. 2015, and references therein). This, in turn, implies that quasar bias increases significantly between redshift 0.5 and 2.5, and that the characteristic mass of the dark matter haloes that host quasars is roughly constant across this redshift range. Myers et al. (2007b) estimated how quasar clustering on small scales changes with redshift using a sample of 91 photometrically classified candidate quasars and found that UV-excess quasars at  $28 h^{-1}$  kpc cluster  $> 5$  times ( $\sim 2\sigma$ ) higher at  $z > 2$  than at  $z < 2$ . However, the evolution of quasar clustering on proper scales of  $< 50 h^{-1}$  kpc has not yet been measured using a *spectroscopically confirmed* sample of quasar pairs, likely because sample sizes have never been sufficiently large to bin by redshift. With the unprecedentedly large number of binary quasars in, and wide redshift range of, our KDE-complete sample, we can make this measurement for the first time.

We divide our KDE-complete sample of quasar pairs into four bins of redshift of similar width ( $\Delta z \simeq 0.46$ ) centered at  $z = 0.67, 1.12, 1.58$  and  $2.03$ . These bins contain 6, 7, 20 and 14 quasar pairs, respectively<sup>11</sup>. We then measure the correlation function  $\bar{W}_p(R_{\min}, R_{\max})$  in each bin of redshift over the full range of proper scales of our sample ( $17.0 < R < 36.2 h^{-1}$  kpc). We plot the results of this analysis in the right-hand panel of Figure 8. Having measured the volume-averaged correlation function in four slices of redshift, we use the method described in §3.2 to derive the amplitude of quasar clustering ( $A$  from Eqn. 8) in each bin of redshift. The left-hand panel of Figure 8 shows the values of  $A$  that correspond to the measured  $\bar{W}_p(z)$  values plotted in the right-hand panel. We measure the clustering amplitude of quasars at  $\sim 25 h^{-1}$  kpc from our full KDE-complete sample of 47 confirmed binaries to be  $A = 24.1 \pm 3.6$  (the pink star in Figure 8).

Croom et al. (2005) measured a clustering amplitude equivalent to  $A \sim 5$  at  $z \sim 1.5$  on Mpc-scales. The fact that we find a factor of  $\sim 4\times$  stronger amplitude for quasar clustering on kpc scales than has been found on Mpc scales suggests that, on small scales, quasar clustering climbs rapidly above the dark matter model (Smith et al. 2003) that we use in Eqn. 5. This was interpreted as an “excess” by Hennawi et al. (2006b) and Myers et al. (2008), perhaps driven by pairs of quasars being fed during galaxy mergers. Hopkins et al. (2007) argued instead that strong quasar clustering on small scales is simply indicative of quasars occupying group-scale or “merger-prone” environments. More recently, the small-scale clustering of quasars has been modeled using the “one-halo” term in the HOD (e.g., Kayo & Oguri 2012; Richardson et al. 2012, 2013). As we argue in §4.1, this “excess” is, in fact, probably close-to-consistent with the amplitude of clustering found for some types of galaxies on small scales.

Our unprecedentedly precise measurements of  $\bar{W}_p$  on scales of  $\sim 25 h^{-1}$  kpc allow us to make a first comparison of the *evolution* of quasar clustering over 3 orders of magnitude in scale. To

<sup>11</sup> Choosing the redshift slices such that they contain the same number of pairs would cause some bins to be very narrow.

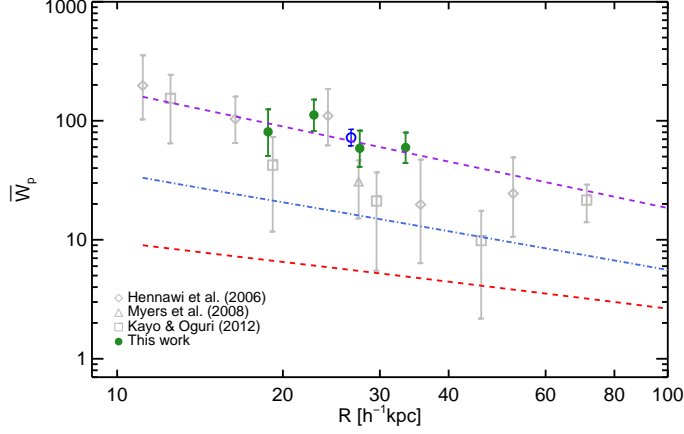


**Figure 7.** The projected correlation function of quasars in four bins of proper scale (filled green circles) as well as the measured correlation function for the full sample at  $\bar{z} = 1.55$  and  $R = 26.6 h^{-1} \text{ kpc}$  (open blue circle). The grey symbols depict similar measurements from previous studies. Where necessary, we have converted the comoving coordinates used in previous measurements to proper coordinates in order to compare with our data. The red and blue dashed and dot-dashed lines are the extrapolation of the  $\bar{W}_p$  correlation function reported on Mpc-scales by Porciani, Magliocchetti & Norberg (2004) with ( $\gamma = 1.53$ ,  $r_0 = 4.8 h^{-1} \text{ cMpc}$ ) and ( $\gamma = 1.8$ ,  $r_0 = 5.4 h^{-1} \text{ cMpc}$ ), respectively. The purple line shows the best fit to the green data points assuming a correlation length of  $r_0 = 5.0 h^{-1} \text{ cMpc}$ . This line has a power-law index of  $\gamma = 1.97 \pm 0.03$  indicating that the correlation function is steeper on kpc-scales than has been estimated for many quasar samples on Mpc-scales (as discussed further in §4.1)

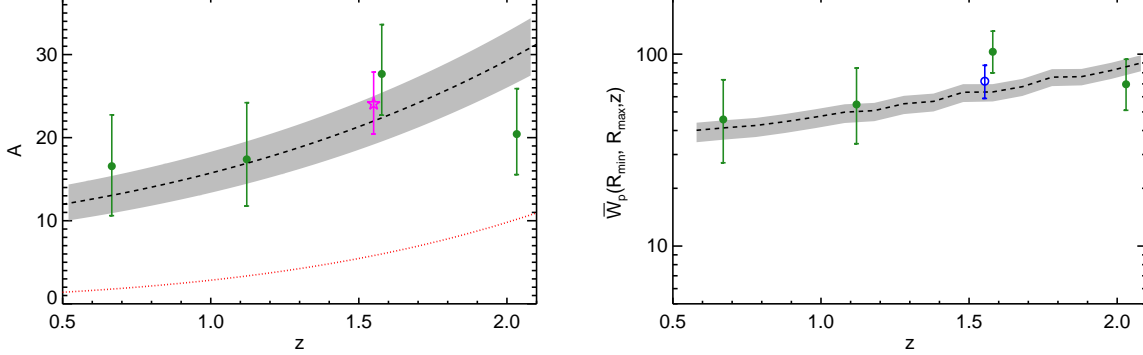


**Figure 8.** Left: Our deduced quasar clustering amplitude at  $R \sim 25 h^{-1} \text{ kpc}$  in each bin of redshift. The pink star depicts the amplitude derived from our measurement of quasar clustering for our full sample ( $A = 24.1 \pm 3.6$ ). The red dotted line is the model for the evolution of quasar bias on Mpc-scales proposed by Croom et al. (2005);  $b_Q^2(z) = (0.53 + 0.289(1+z)^2)^2$ . The black dashed line depicts the best-fit value we find for a one-parameter fit of  $A(z) = (c + 0.289(1+z)^2)^2$ , which is  $c = 2.81 \pm 0.31$ . The grey envelope depicts the  $1\text{-}\sigma$  confidence interval for the fitted parameter  $c$ . Right: The projected correlation function of quasars in four bins of redshift. Each redshift bin spans the full range of proper scales of our KDE-complete sample ( $17.0 \leq R \leq 36.2 h^{-1} \text{ kpc}$ ). The black dashed line is the calculated  $\bar{W}_p$  for the full redshift range of our KDE-complete sample, using the model from the left-hand panel. The grey envelope is the translation of the confidence intervals from the left-hand panel based on the relationship between  $A$  and  $\bar{W}_p$  outlined in §3.2.

do so, we compare our measurements to the empirical description of the evolution of quasar clustering derived by Croom et al. (2005) over scales of  $1 < s < 25 h^{-1} \text{ cMpc}$ . Using our empirical formalism from Eqn. 8, Croom et al. (2005) found the equivalent of  $A(z) = [0.53 + 0.289(1+z)^2]^2$ . Our goal is to compare the evolution of the amplitude of quasar clustering on kpc- and Mpc-scales. Because we measure a larger amplitude ( $A$ ) on kpc-scales than is found on Mpc-scales, we allow the offset in the Croom et al. (2005) empirical description to float and fit a model of the form  $A = [c + 0.289(1+z)^2]^2$ . We find a best fit of  $c = 2.81 \pm 0.31$  to our measurements in four slices of redshift

over the range  $0.43 < z < 2.26$ , which we plot in (both panels of) Figure 8. We find that the evolution of the amplitude of quasar clustering on kpc-scales across a wide range of redshift, is in reasonable agreement with the overall Mpc-scale empirical description of Croom et al. (2005), once we account for the amplitude offset of a factor of  $\sim 4\times$ . The  $\chi^2$  value of our best fit is 4.2, which is only rejected at a confidence-level of 12%. Based on our, admittedly highly empirical model of Eqn. 8, this suggests that the evolution of the amplitude of quasar clustering on the smallest scales can be adequately modeled using descriptions of quasar evolution on Mpc-scales.

## 5 SUMMARY AND CONCLUSIONS

We present by far the largest sample of spectroscopically confirmed binary quasars with proper transverse separations of  $17.0 \leq R \leq 36.2 h^{-1}$  kpc. Our sample, which is  $\sim 6\times$  larger than any previous homogeneously selected sample on these proper scales, is derived from SDSS imaging over an area corresponding to SDSS DR6. Our quasars are targeted using a Kernel Density Estimation technique (KDE), and confirmed using long-slit spectroscopy on a range of facilities. We derive a statistically complete sub-sample of 47 binary quasars with  $g < 20.85$ , which extends across angular scales of  $2.9'' < \Delta\theta < 6.3''$  and redshifts of  $0.43 < z < 2.26$ . This sample is targeted from a parent catalogue that would be equivalent to a full spectroscopic survey of nearly 360,000 quasars.

We determine the projected correlation function ( $\bar{W}_p$ ) of  $0.43 < z < 2.26$  quasars over proper transverse scales of  $17.0 \leq R \leq 36.2 h^{-1}$  kpc, in four bins of scale. We find that quasars cluster on kpc-scales far higher than implied by a  $\gamma = 1.8$  power-law, as has been adopted by some authors on Mpc-scales (e.g. Porciani, Magliocchetti & Norberg 2004). For  $r_0 = 5 h^{-1}$  cMpc, we find that a power-law slope of  $\gamma = 1.97 \pm 0.03$  is therefore required to fit quasar clustering on proper scales of  $R \sim 25 h^{-1}$  kpc. This is steeper than what is typically measured for galaxies, but is consistent with some measurements of galaxy clustering, particularly on very small scales and at  $z > 0.5$ . We therefore confirm previous results that suggest that the steep shape of quasar clustering on small scales may be indicative of quasars “turning on” in galaxy mergers (e.g. Hennawi et al. 2006b; Myers et al. 2008) or of quasars inhabiting group-scale (“merger-prone”) environments (e.g. Hopkins et al. 2007). The  $\gamma \sim 2$  power-law we find is also consistent with results that suggest that quasars require a steeper power-law index than is typical for popular theoretical dark matter density relations (e.g. Moore et al. 1996; Navarro, Frenk & White 1997). A full modeling of this effect will require an in-depth study of the “one-halo” term of the HOD (e.g., Kayo & Oguri 2012; Richardson et al. 2012, 2013), which we reserve for future work.

Our sample of binary quasars is the first that is sufficiently large to study quasar clustering as a function of redshift on proper scales of  $R \sim 25 h^{-1}$  kpc. To investigate the evolution of quasar clustering on small scales, we measure the projected quasar correlation function in four bins of redshift over  $0.4 \leq z \leq 2.3$  and derive the amplitude of quasar clustering on small scales. We find that, at  $z \sim 1.5$ , the clustering of quasars substantially exceeds our chosen dark matter model (Smith et al. 2003), and does so by a factor of about 4 in amplitude as compared to the excess-over-dark-matter on Mpc-scales.

We compare the evolution of the amplitude of quasar clustering on proper scales of  $R \sim 25 h^{-1}$  kpc to empirical relationships derived by Croom et al. (2005) on scales of  $\sim 10 h^{-1}$  Mpc. Our kpc-scale results cannot rule out descriptions of the evolution of quasar clustering on Mpc-scales, which, at its simplest would imply that the dark matter in which quasars are embedded evolves similarly to the baryonic matter over 3 orders of magnitude in scale. However, our sample size is too small and our modeling is too physically simplistic to formally detect a strong evolution in quasar bias from  $z \sim 0.5$  to  $z \sim 2.5$ , which leaves open the possibility that how the clustering of quasars evolves with redshift may be a function of scale.

## ACKNOWLEDGMENTS

SE and ADM were partially supported by the National Science Foundation (NSF) through grant number 1515404. SGD, AAM, and MJG acknowledge partial support from NSF grants AST-1313422, AST-1413600, and AST-1518308. We thank the staff of Palomar Observatory for their assistance during our observing runs. Observations reported here were obtained at; (1) the MMT Observatory, a joint facility of the Smithsonian Institution and the University of Arizona; (2) the Hale Telescope, Palomar Observatory as part of a continuing collaboration between the California Institute of Technology, NASA/JPL, Oxford University, Yale University, and the National Astronomical Observatories of China; and (3) the Mayall telescope at Kitt Peak National Observatory, National Optical Astronomy Observatory (NOAO Prop. ID: 2008A-0127; PI: Myers), which is operated by the Association of Universities for Research in Astronomy (AURA) under cooperative agreement with the National Science Foundation. The authors are honored to be permitted to conduct astronomical research on Iolkam Du’ag (Kitt Peak), a mountain with particular significance to the Tohono O’odham. This work used the facilities of The Advanced Research Computing Center at the University of Wyoming (Advanced Research Computing Center. 2012. Mount Moran: IBM System X cluster. Laramie, WY: University of Wyoming. <http://n2t.net/ark:/85786/m4159c>).

## REFERENCES

- Abazajian K. et al., 2003, *AJ*, 126, 2081  
 Adelman-McCarthy J. K. et al., 2008, *ApJS*, 175, 297  
 Berlind A. A., Weinberg D. H., 2002, *ApJ*, 575, 587  
 Blanton M. R., Lin H., Lupton R. H., Maley F. M., Young N., Zehavi I., Loveday J., 2003, *AJ*, 125, 2276  
 Chatterjee S., Degraf C., Richardson J., Zheng Z., Nagai D., Di Matteo T., 2012, *MNRAS*, 419, 2657  
 Chatterjee S., Nguyen M. L., Myers A. D., Zheng Z., 2013, *ApJ*, 779, 147  
 Coil A. L., Hennawi J. F., Newman J. A., Cooper M. C., Davis M., 2007, *ApJ*, 654, 115  
 Coil A. L., Mendez A. J., Eisenstein D. J., Moustakas J., 2016, *ArXiv:1609.09090*  
 Cole S., Kaiser N., 1989, *MNRAS*, 237, 1127  
 Crampton D., Cowley A. P., Hickson P., Kindl E., Wagner R. M., Tyson J. A., Gullixson C., 1988, *ApJ*, 330, 184  
 Croom S. M. et al., 2005, *MNRAS*, 356, 415  
 Croom S. M. et al., 2009, *MNRAS*, 399, 1755  
 Croom S. M., Shanks T., 1996, *MNRAS*, 281, 893  
 Croom S. M., Smith R. J., Boyle B. J., Shanks T., Miller L., Outram P. J., Loaring N. S., 2004, *MNRAS*, 349, 1397  
 Dawson K. S. et al., 2013, *AJ*, 145, 10  
 Di Matteo T., Springel V., Hernquist L., 2005, *Nature*, 433, 604  
 Djorgovski S., 1991, in *Astronomical Society of the Pacific Conference Series*, Vol. 21, *The Space Distribution of Quasars*, Crampton D., ed., pp. 349–353  
 Djorgovski S., Perley R., Meylan G., McCarthy P., 1987, *ApJ*, 321, L17  
 Djorgovski S., Spinrad H., 1984, *ApJ*, 282, L1  
 Eftekharzadeh S. et al., 2015, *MNRAS*, 453, 2779  
 Ellison S. L., Mendel J. T., Scudder J. M., Patton D. R., Palmer M. J. D., 2013, *MNRAS*, 430, 3128  
 Ellison S. L., Patton D. R., Mendel J. T., Scudder J. M., 2011, *MNRAS*, 418, 2043

- Fan X. et al., 1999, *ApJ*, 526, L57  
 Fan X. et al., 2006, *AJ*, 131, 1203  
 Favole G. et al., 2016, *MNRAS*, 461, 3421  
 Gehrels N., 1986, *ApJ*, 303, 336  
 Green P. J., Myers A. D., Barkhouse W. A., Aldcroft T. L., Trichas M., Richards G. T., Ruiz Á., Hopkins P. F., 2011, *ApJ*, 743, 81  
 Gregg M. D., Becker R. H., White R. L., Richards G. T., Chaffee F. H., Fan X., 2002, *ApJ*, 573, L85  
 Hagen H.-J., Hopp U., Engels D., Reimers D., 1996, *A&A*, 308, L25  
 Hennawi J. F. et al., 2010, *ApJ*, 719, 1672  
 Hennawi J. F., Prochaska J. X., 2013, *ApJ*, 766, 58  
 Hennawi J. F. et al., 2006a, *ApJ*, 651, 61  
 Hennawi J. F. et al., 2006b, *AJ*, 131, 1  
 Hewett P. C., Foltz C. B., Harding M. E., Lewis G. F., 1998, *AJ*, 115, 383  
 Hewett P. C., Webster R. L., Harding M. E., Jedrzejewski R. J., Foltz C. B., Chaffee F. H., Irwin M. J., Le Fevre O., 1989, *ApJ*, 346, L61  
 Hopkins P. F., Hernquist L., Cox T. J., Kereš D., 2008, *ApJS*, 175, 356  
 Hopkins P. F., Lidz A., Hernquist L., Coil A. L., Myers A. D., Cox T. J., Spergel D. N., 2007, *ApJ*, 662, 110  
 Hopkins P. F., Somerville R. S., Hernquist L., Cox T. J., Robertson B., Li Y., 2006, *ApJ*, 652, 864  
 Inada N. et al., 2008, *AJ*, 135, 496  
 Inada N. et al., 2010, *AJ*, 140, 403  
 Inada N. et al., 2012, *AJ*, 143, 119  
 Jiang N., Wang H., Mo H., Dong X., Wang T., Zhou H., 2016, *ArXiv:1602.08825*  
 Kaiser N., 1984, *ApJ*, 284, L9  
 Kayo I., Oguri M., 2012, *MNRAS*, 424, 1363  
 Kochanek C. S., Falco E. E., Muñoz J. A., 1999, *ApJ*, 510, 590  
 Lacey C., Cole S., 1993, *MNRAS*, 262, 627  
 Masjedi M. et al., 2006, *ApJ*, 644, 54  
 McCarthy P. J., Dickinson M., Filippenko A. V., Spinrad H., van Breugel W. J. M., 1988, *ApJ*, 328, L29  
 McGreer I. D., Eftekharzadeh S., Myers A. D., Fan X., 2016, *AJ*, 151, 61  
 Meylan G., Djorgovski S., 1989, *ApJ*, 338, L1  
 Meylan G., Djorgovski S., Weir N., Shaver P., 1990, *The Messenger*, 59, 47  
 Miller L., Lopes A. M., Smith R. J., Croom S. M., Boyle B. J., Shanks T., Outram P., 2004, *MNRAS*, 348, 395  
 Moore B., Katz N., Lake G., Dressler A., Oemler A., 1996, *Nature*, 379, 613  
 Mortlock D. J., Webster R. L., Francis P. J., 1999, *MNRAS*, 309, 836  
 Muñoz J. A., Falco E. E., Kochanek C. S., Lehár J., Herold L. K., Fletcher A. B., Burke B. F., 1998, *ApJ*, 492, L9  
 Myers A. D., Brunner R. J., Nichol R. C., Richards G. T., Schneider D. P., Bahcall N. A., 2007a, *ApJ*, 658, 85  
 Myers A. D., Brunner R. J., Richards G. T., Nichol R. C., Schneider D. P., Bahcall N. A., 2007b, *ApJ*, 658, 99  
 Myers A. D. et al., 2006, *ApJ*, 638, 622  
 Myers A. D., Richards G. T., Brunner R. J., Schneider D. P., Strand N. E., Hall P. B., Blomquist J. A., York D. G., 2008, *ApJ*, 678, 635  
 Navarro J. F., Frenk C. S., White S. D. M., 1997, *ApJ*, 490, 493  
 Oguri M. et al., 2006, *AJ*, 132, 999  
 Oguri M. et al., 2012, *AJ*, 143, 120  
 Oguri M. et al., 2008, *AJ*, 135, 512  
 Oke J. B., Gunn J. E., 1983, *ApJ*, 266, 713  
 Padmanabhan N., White M., Norberg P., Porciani C., 2009, *MNRAS*, 397, 1862  
 Pâris I. et al., 2016, *ArXiv:1608.06483*  
 Peebles P. J. E., 1973, *ApJ*, 185, 413  
 Pindor B. et al., 2006, *AJ*, 131, 41  
 Pindor B., Turner E. L., Lupton R. H., Brinkmann J., 2003, *AJ*, 125, 2325  
 Planck Collaboration et al., 2015, *ArXiv:1502.01589*  
 Porciani C., Magliocchetti M., Norberg P., 2004, *MNRAS*, 355, 1010  
 Porciani C., Norberg P., 2006, *MNRAS*, 371, 1824  
 Prochaska J. X. et al., 2013, *ApJ*, 776, 136  
 Prochaska J. X., Lau M. W., Hennawi J. F., 2014, *ApJ*, 796, 140  
 Richards G. T. et al., 2002, *AJ*, 123, 2945  
 Richards G. T. et al., 2009, *ApJS*, 180, 67  
 Richards G. T. et al., 2004, *ApJS*, 155, 257  
 Richardson J., Chatterjee S., Zheng Z., Myers A. D., Hickox R., 2013, *ApJ*, 774, 143  
 Richardson J., Zheng Z., Chatterjee S., Nagai D., Shen Y., 2012, *ApJ*, 755, 30  
 Ross N. P. et al., 2009, *ApJ*, 697, 1634  
 Schlegel D. J., Finkbeiner D. P., Davis M., 1998, *ApJ*, 500, 525  
 Schneider D. P. et al., 2000, *AJ*, 120, 2183  
 Schneider D. P. et al., 2007, *AJ*, 134, 102  
 Schneider D. P. et al., 2005, *AJ*, 130, 367  
 Schneider D. P. et al., 2010, *AJ*, 139, 2360  
 Schneider D. P., Schmidt M., Gunn J. E., 1994, *AJ*, 107, 1245  
 Shanks T., Boyle B. J., 1994, *MNRAS*, 271, 753  
 Shanks T., Fong R., Boyle B. J., Peterson B. A., 1987, *MNRAS*, 227, 739  
 Sheinis A. I., Bolte M., Epps H. W., Kibrick R. I., Miller J. S., Radovan M. V., Bigelow B. C., Sutin B. M., 2002, *PASP*, 114, 851  
 Shen Y. et al., 2007, *AJ*, 133, 2222  
 Shen Y. et al., 2009, *ApJ*, 697, 1656  
 Smith R. E. et al., 2003, *MNRAS*, 341, 1311  
 Sramek R. A., Weedman D. W., 1978, *ApJ*, 221, 468  
 Stoughton C. et al., 2002, *AJ*, 123, 485  
 Swanson M. E. C., Tegmark M., Blanton M., Zehavi I., 2008, *MNRAS*, 385, 1635  
 Tegmark M., Blanton M. R., Strauss M. A., Hoyle F., Schlegel D., SDSS Collaboration, 2004, *ApJ*, 606, 702  
 Watson D. F., Berlind A. A., McBride C. K., Masjedi M., 2010, *ApJ*, 709, 115  
 Weedman D. W., Weymann R. J., Green R. F., Heckman T. M., 1982, *ApJ*, 255, L5  
 Wetzel A. R., Cohn J. D., White M., 2009, *MNRAS*, 394, 2182  
 White M. et al., 2012, *MNRAS*, 424, 933  
 Wyithe J. S. B., Loeb A., 2005, *ApJ*, 621, 95  
 Zehavi I. et al., 2011, *ApJ*, 736, 59  
 Zhai Z. et al., 2016, *ArXiv:1607.05383*  
 Zhdanov V. I., Surdej J., 2001, *A&A*, 372, 1

Table 5: Candidate quasar pairs drawn from our parent sample <sup>12</sup>.

$\Delta\theta$ (")	Obs. Stat.	$\alpha$ (J2000)	$\delta$ (J2000)	$i$	$g$	Classification	$z_{\text{spec}}$	QQ?
1.449	2	184.19140	35.49488	19.88	20.40	Q	-1	4
	2	184.19190	35.49486	19.08	19.39	Q	2.013	
1.693	2	204.77974	13.17768	18.91	19.03	Q	2.241	4
	2	204.78015	13.17741	18.87	18.96	Q	2.237	
1.762	0	19.55013	-1.07848	19.99	21.00	U	0.740	1
	0	19.55053	-1.07820	20.35	20.40	U	-1	
1.897	0	177.82866	46.87642	20.28	20.68	U	-1	1
	0	177.82939	46.87626	19.04	20.41	U	-1	
1.939	0	230.20850	26.62804	19.07	19.35	Q	-1	1
	2	230.20911	26.62802	19.00	19.21	Q	1.365	
1.999	2	228.91032	15.19300	18.37	18.70	Q	2.052	4
	2	228.91080	15.19331	18.05	18.16	Q	2.054	
2.102	0	112.11562	26.11704	19.65	19.98	U	-1	1
	0	112.11615	26.11737	18.84	18.90	U	-1	
2.173	0	146.32053	22.41586	20.79	20.94	U	-1	1
	0	146.32063	22.41646	20.72	20.81	U	-1	
2.196	0	250.07547	10.75175	19.59	20.42	U	-1	1
	0	250.07599	10.75141	17.83	18.39	U	-1	
2.267	0	244.24273	36.50716	20.42	20.17	U	-1	1
	0	244.24332	36.50758	20.40	20.12	U	-1	
2.316	2	250.79727	31.93844	19.53	20.00	Q	0.587	1
	0	250.79745	31.93907	19.47	19.89	U	-1	
2.453	2	145.64575	23.17533	19.76	19.91	Q	1.833	3
	2	145.64598	23.17468	19.70	19.80	Q	1.833	
2.654	2	158.83012	7.88232	20.16	20.62	Q	1.218	3
	2	158.83069	7.88278	19.02	19.10	Q	1.215	
2.678	0	161.08777	4.49745	20.60	20.99	U	-1	1
	0	161.08844	4.49713	19.35	19.73	U	-1	
2.695	0	115.60587	24.86230	20.64	20.90	U	-1	1
	0	115.60665	24.86254	20.56	20.74	U	-1	
2.829	1	182.49029	11.61649	20.46	20.76	Q	0.899	3
	1	182.49049	11.61573	20.40	20.65	Q	0.904	
2.868	0	322.49351	12.00661	20.71	20.88	S	-1	1
	0	322.49390	12.00731	20.50	20.49	U	-1	
2.903	2	227.17583	33.46739	20.60	20.44	Q	0.877	3
	1	227.17590	33.46820	20.56	20.38	Q	0.878	
2.912	1	152.07303	17.25558	20.27	20.67	Q	1.087	3
	1	152.07367	17.25506	20.19	20.52	Q	1.083	
2.918	1	143.15840	29.40301	20.94	20.66	U	-1	1
	0	143.15854	29.40221	20.90	20.59	U	-1	
2.925	2	150.36812	50.46623	17.71	18.34	Q	1.845	4
	2	150.36922	50.46581	17.32	17.55	Q	1.841	
2.933	1	158.41804	2.47517	19.65	20.28	U	-1	1
	1	158.41884	2.47531	19.91	20.14	Q	1.833	
2.993	2	207.37436	12.45193	18.73	19.32	Q	1.722	4
	1	207.37503	12.45245	18.66	19.19	Q	1.722	

1) Angular separation of the two members of the pair; 2) The observational status of the pair is “0” if there is insufficient information to determine the redshift of a candidate, “1” for sources confirmed by this study, and “2” for sources confirmed in previous studies (Schneider et al. 2005; Hennawi et al. 2006b; Inada et al. 2008; Myers et al. 2008; Oguri et al. 2008; Schneider et al. 2010; Oguri et al. 2012; Prochaska et al. 2013; Prochaska, Lau & Hennawi 2014; Pâris et al. 2016); 3-4) Source coordinates in degrees; 5-6) dereddened  $i$ - and  $g$ -magnitudes; 7) Spectroscopic classification: Q=Quasar G=Galaxy, S=Star, U=No Spectrum, NQ=A spectrum exists but it did not yield a definitive classification (i.e “Not a quasar”); 8) The measured or reported spectroscopic redshift for the members, -1 for objects with no redshift; 9) Classification of the pair as (1) lacking sufficient spectroscopic information to define its nature, (2) a projected pair (star-star, star-quasar, two quasars at different redshifts etc.), (3) a binary quasar, (4) a gravitational lens.

<sup>12</sup> The full table is available in the electronic version of this paper.

Table 6: Complete sample of 47 spectroscopically confirmed binaries

Name	<i>R.A.</i> (J2000)	<i>Dec.</i> (J2000)	<i>g</i>	<i>i</i>	$\Delta\theta$ ( $''$ )	$z_{\text{spec}}$	$ \Delta v $ ( $\text{km s}^{-1}$ )	<i>R</i> ( $h^{-1}$ kpc)
SDSS J0718+4020 A	109.51462	40.35075	20.04	20.16	5.926	1.838	0	34.6
SDSS J0718+4020 B	109.51288	40.34978	20.66	21.07				
SDSS J0751+1303 A	117.76192	13.06113	20.31	20.82	6.166	1.545	1300	36.1
SDSS J0751+1303 B	117.76159	13.05944	20.38	20.94				
SDSS J0813+5416 A	123.30461	54.27972	17.27	17.24	5.042	0.778	200	26.1
SDSS J0813+5416 B	123.30266	54.28054	20.20	20.25				
SDSS J0818+3623 A	124.63308	36.38616	17.73	17.99	6.094	1.961	0	35.3
SDSS J0818+3623 B	124.63222	36.38770	19.26	19.75				
SDSS J0846+2709 A	131.60213	27.16733	20.44	20.43	4.637	2.195	0	26.5
SDSS J0846+2709 B	131.60140	27.16622	20.46	20.66				
SDSS J0916+3252 A	139.24397	32.87321	19.38	19.73	6.122	1.911	600	35.6
SDSS J0916+3252 B	139.24195	32.87304	19.75	20.10				
SDSS J0922-0117 A	140.57307	-1.29715	18.64	18.93	6.032	1.677	1400	35.3
SDSS J0922-0117 B	140.57305	-1.29883	19.48	19.83				
SDSS J0954+1920 A	148.62408	19.33632	18.41	18.58	4.376	1.744	0	25.6
SDSS J0954+1920 B	148.62282	19.33660	19.96	20.29				
SDSS J0959+5449 A	149.78113	54.81844	19.74	20.04	3.945	1.956	200	22.9
SDSS J0959+5449 B	149.77942	54.81892	20.29	20.61				
SDSS J1048+0950 A	162.19373	9.83695	20.56	20.74	4.447	1.666	0	26.1
SDSS J1048+0950 B	162.19254	9.83652	20.61	20.84				
SDSS J1145+2857 A	176.26947	28.95353	19.97	20.24	4.085	2.173	100	23.4
SDSS J1145+2857 B	176.26818	28.95363	20.55	20.63				
SDSS J1145+2857 A	176.93478	33.08547	17.47	17.58	4.691	1.164	1000	26.9
SDSS J1145+2857 B	176.93325	33.08565	20.14	20.18				
SDSS J1158+1355 A	179.71272	13.92666	20.78	20.66	3.237	2.062	1800	18.7
SDSS J1158+1355 B	179.71198	13.92718	20.85	20.78				
SDSS J1207+1408 A	181.86359	14.13900	19.97	20.11	3.949	1.795	500	23.1
SDSS J1207+1408 B	181.86292	14.13811	20.03	20.37				
SDSS J1215+0225 A	183.94466	2.43279	19.51	19.69	5.729	1.445	0	33.5
SDSS J1215+0225 B	183.94425	2.43125	19.55	19.77				
SDSS J1219+2541 A	184.89709	25.68951	19.61	19.87	5.897	1.596	200	34.6
SDSS J1219+2541 B	184.89556	25.68862	18.64	20.07				
SDSS J1235+0434 A	188.98030	68.60752	19.51	19.64	3.513	1.529	1800	20.6
SDSS J1235+0434 B	188.97826	68.60689	19.54	19.72				
SDSS J1259+1241 A	194.98174	12.69828	19.73	19.99	3.554	2.180	900	20.3
SDSS J1259+1241 B	194.98110	12.69752	19.78	20.09				
SDSS J1303+5100 A	195.85907	51.01311	19.98	20.33	3.806	1.686	200	22.3
SDSS J1303+5100 B	195.85893	51.01417	20.34	20.54				
SDSS J1320+3056 A	200.09435	30.93842	19.65	19.90	4.745	1.597	500	27.8
SDSS J1320+3056 B	200.09394	30.93969	19.68	19.94				

Continued on next page.

Table 6 – continued from previous page

Name	<i>R.A.</i> (J2000)	<i>Dec.</i> (J2000)	<i>g</i>	<i>i</i>	$\Delta\theta$ (")	$z_{\text{spec}}$	$ \Delta v $ (km s <sup>-1</sup> )	<i>R</i> (h <sup>-1</sup> kpc)
SDSS J1337+6012 A	204.30472	60.20183	18.34	18.55	3.118	1.721	1500	18.2
SDSS J1337+6012 B	204.30452	60.20269	19.70	20.05				
SDSS J1339+6208 A	204.75824	62.14766	19.96	20.26	3.89	1.799	1800	22.7
SDSS J1339+6208 B	204.75796	62.14659	20.36	20.90				
SDSS J1344+1948 A	206.12888	19.81089	19.95	20.06	4.694	1.534	200	27.5
SDSS J1344+1948 B	206.12883	19.80959	20.25	20.48				
SDSS J1418+2441 A	214.73140	24.68464	19.83	20.15	4.504	0.573	400	20.5
SDSS J1418+2441 B	214.73091	24.68581	19.87	20.23				
SDSS J1426+0719 A	216.51802	7.32501	19.82	20.03	4.271	1.324	300	24.8
SDSS J1426+0719 B	216.51778	7.32385	20.59	20.82				
SDSS J1430+0714 A	217.51202	7.23648	19.02	19.39	5.414	1.245	1700	31.3
SDSS J1430+0714 B	217.51110	7.23767	19.74	20.27				
SDSS J1430+1539 A	217.51620	15.66371	19.76	19.64	6.265	0.912	200	34.0
SDSS J1430+1539 B	217.51486	15.66256	19.75	20.06				
SDSS J1431+2705 A	217.77074	27.09129	20.10	20.19	5.913	2.261	900	33.6
SDSS J1431+2705 B	217.76937	27.09018	20.13	20.25				
SDSS J1433+1450 A	218.46286	14.83489	19.21	19.38	3.336	1.506	500	19.5
SDSS J1433+1450 B	218.46227	14.83561	19.25	19.45				
SDSS J1439+0601 A	219.95763	6.01756	20.39	20.80	5.329	1.151	0	30.4
SDSS J1439+0601 B	219.95697	6.01889	20.47	20.94				
SDSS J1440+1515 A	220.24983	15.26339	19.55	19.97	3.852	1.153	0	22.0
SDSS J1440+1515 B	220.24968	15.26233	20.48	20.65				
SDSS J1444+5413 A	221.09413	54.22240	20.05	20.25	3.446	1.584	0	20.2
SDSS J1444+5413 B	221.09255	54.22263	20.15	20.83				
SDSS J1457+2516 A	224.49562	25.28052	19.71	19.82	5.689	1.376	0	33.2
SDSS J1457+2516 B	224.49422	25.27957	19.82	19.99				
SDSS J1458+5448 A	224.61137	54.80367	19.62	20.49	5.142	1.905	300	29.9
SDSS J1458+5448 B	224.60902	54.80413	20.47	20.80				
SDSS J1507+2903 A	226.94681	29.05924	19.86	19.88	4.349	0.863	0	23.2
SDSS J1507+2903 B	226.94545	29.05949	20.19	20.44				
SDSS J1512+2951 A	228.24347	29.86401	18.38	18.58	5.312	1.809	500	31.0
SDSS J1512+2951 B	228.24194	29.86337	19.52	20.83				
SDSS J1518+2959 A	229.59763	29.99099	19.87	20.17	5.281	1.249	800	30.5
SDSS J1518+2959 B	229.59607	29.99042	19.92	20.25				
SDSS J1530+5304 A	232.66176	53.06685	20.28	20.64	4.114	1.535	200	24.1
SDSS J1530+5304 B	232.66068	53.06779	20.31	20.70				
SDSS J1545+2755 A	236.31659	27.93363	19.43	19.70	3.735	1.494	100	21.9
SDSS J1545+2755 B	236.31556	27.93314	20.24	20.66				
SDSS J1553+2230 A	238.37730	22.50399	20.50	20.70	6.111	0.641	1300	29.2
SDSS J1553+2230 B	238.37596	22.50284	20.63	20.93				
SDSS J1559+2640 A	239.78497	26.67552	19.66	19.81	5.367	0.870	1000	28.7
SDSS J1559+2640 B	239.78424	26.67686	20.29	20.44				

Continued on next page.

**Table 6 – continued from previous page**

Name	<i>R.A.</i> (J2000)	<i>Dec.</i> (J2000)	<i>g</i>	<i>i</i>	$\Delta\theta$ ( $''$ )	$z_{\text{spec}}$	$ \Delta v $ ( $\text{km s}^{-1}$ )	<i>R</i> ( $h^{-1}$ kpc)
SDSS J1602+1314 A	240.61542	13.23796	19.93	20.08	5.324	2.018	100	30.8
SDSS J1602+1314 B	240.61448	13.23680	20.35	20.46				
SDSS J1606+2900 A	241.51259	29.01413	18.37	18.29	3.446	0.770	300	17.7
SDSS J1606+2900 B	241.51172	29.01355	18.36	18.50				
SDSS J1635+2911 A	248.79294	29.18783	20.11	20.33	4.917	1.587	0	28.8
SDSS J1635+2911 B	248.79228	29.18907	20.16	20.42				
SDSS J1637+2636 A	249.25389	26.60274	18.97	19.11	3.904	1.961	0	22.6
SDSS J1637+2636 B	249.25367	26.60381	20.52	20.60				
SDSS J1649+1733 A	252.37083	17.55239	19.23	19.45	3.618	2.080	0	20.8
SDSS J1649+1733 B	252.36997	17.55182	19.42	19.77				
SDSS J1723+5904 A	260.82260	59.07956	18.56	18.78	3.721	1.597	400	21.8
SDSS J1723+5904 B	260.82211	59.07855	20.07	20.32				

Columns: 1) Name of the members of the binary, where the brighter and fainter quasars in the pair in *g*-band are referred to as “A” or “B” respectively; 2 – 3) Right Ascension and Declination of each quasar; 4 – 5) *g*- and *i*-magnitude of each quasar; 6) Angular separation of the quasars in the binary; 7) Spectroscopic redshift for the binary; 8) The velocity difference between the quasars in the binary; 9) The transverse proper separation between the quasars in the binary.